PERGAMON

Journal of Quantitative Spectroscopy & Radiative Transfer 64 (2000) 87–107

Journal of Quantitative Spectroscopy & Radiative Transfer

www.elsevier.com/locate/jqsrt

Note

Theoretical study of the collision-induced fundamental absorption spectra of O_2–O_2 pairs for temperatures between 193 and 273 K

G. Moreau[a], J. Boissoles[a], C. Boulet[b], R.H. Tipping[c,*], Q. Ma[d]

[a] *Unité Mixte de Recherche P.A.L.M.S. (Physique des Atomes, Lasers, Molécules, et Surfaces), Université de Rennes I, Campus de Beaulieu, 35042, Rennes Cedex, France*

[b] *Laboratoire de Physique Moléculaire et Applications, CNRS, Université de Paris-Sud, Campus d'Orsay 91405, Orsay Cedex, France*

[c] *Department of Physics and Astronomy, University of Alabama, Tuscaloosa, AL 35487, USA*

[d] *Department of Applied Physics, Columbia University, and Institute for Space Studies, Goddard Space Flight Center, 2880 Broadway, New York, NY, USA*

Received 13 July 1998

Abstract

A theoretical analysis of the collision-induced fundamental absorption spectra of O_2–O_2 pairs is presented for temperatures between 193 and 273 K. Most of the absorption arises from the long-range quadrupole and hexadecapole-induced dipole mechanisms for which accurate matrix elements are available from various other experimental measurements or from ab initio calculations. The line shape used is that obtained from quantum computations of the far infrared collision-induced absorption of N_2, modified to include dips resulting from the effects of intercollisional interference. Several refinements, including contributions from back-reaction and short-range induced-dipole moments, can improve the agreement in certain spectral regions but do not lead to significant improvement in the global fits to the experimental data. The small structural features superimposed on the smooth continuum can be modeled by the modified line shape but the half-widths of the dips have a density dependence inconsistent with that arising from interference. On the other hand, difference spectra obtained by subtracting the theoretical results from the experimental data appear quite similar to those obtained previously at low temperatures, leading to the conclusion that this structure is due to dimers. Further experimental results at higher temperatures and for O_2–N_2 pairs would be useful to validate this interpretation.

*Corresponding author. E-mail: rtipping@bama.ua.edu

0022-4073/99/$-see front matter
PII: S0022-4073(98)00141-1

1. Introduction

The collision-induced fundamental band of oxygen is important from an historical as well as a practical viewpoint. This was the system in which collision-induced spectra were first identified by Welsh and co-workers in 1949 [1]. For an overview of this type of absorption mechanism, the reader is referred to the excellent monograph by Frommhold [2]. Since its discovery, there have been a number of laboratory studies, and references to earlier work can be found in the bibliographies of Rich and McKellar [3] and Hunt and Poll [4]. Much later, the collision- induced fundamental band of O_2 was detected in long-path measurements through the stratosphere [5].

In a previous paper [6], we studied theoretically the collision-induced fundamental band of N_2–N_2 pairs. In particular, we showed that one could achieve reasonable agreement over a range of temperatures by considering only the long-range quadrupolar and hexadecapolar mechanisms using existing data for the various matrix elements of the multipole moments and polarizabilities. Recently, however, more accurate measurements of N_2–N_2 in the temperature range 230–300 K by Lafferty et al. [7] revealed a weak structure superimposed on the broad continuum; this structure appears as small dips at the Raman frequencies of the lines. Such structure had been seen earlier in low-temperature (77–90 K) fundamental spectra [8] and very recently in the pure rotational region [9], where it was attributed to van der Waal dimers. However, it was somewhat surprising that this structure persists with appreciable magnitude to 300 K.

Similar structure has also been observed in the fundamental O_2–O_2 spectra [10, 11], where it is actually more apparent because the lines are farther apart. This separation arises even though the rotational constant B_e is smaller for O_2 than for N_2 because of nuclear statistical weights; in O_2, alternate lines are missing, while in N_2 there is a 2:1 ratio between even and odd J levels.

In Ref. [7], two possible alternative theoretical explanations for the dips were mentioned: intercollisional dips [12] that are well known in Q lines of H_2, and line-mixing effects [13]. The intercollisional dips occur at the line centers and have been attributed to short-range isotropic overlap dipoles, although a dip was observed in the $S_1(0)$ line in H_2–He mixtures [14]. Line-mixing, on the other hand, would play a role at all temperatures, but, in general, would not result in dips at the line center frequencies.

In an attempt to understand this structure, theoretical modeling of the O_2–O_2 fundamental spectra has been carried out and the results presented in the present paper. In Section 2, we review the theoretical long-range mechanisms considered previously and include three additional "back reaction" mechanisms [15]; although the latter are weaker by approximately two orders of magnitude, they have the same angular symmetries as the isotropic and an isotropic overlap mechanisms. We then introduce a short-range dependence for all the induced-dipole components. The line shape used, with and without a parameterized intercollisional dip in order to represent the effect of intercollisional interference, is discussed briefly in Section 3. In Section 4, we discuss the best values found in the literature for the quadrupole, hexadecapole, and polarizability matrix elements used in the calculations. In Section 5, we present results for comparisons with experimental data, and we illustrate the sensitivity of these results for small changes in the matrix elements, line shapes, and other fitting parameters. Our conclusions are discussed in Section 6.

2. Theory of collision-induced spectra of O_2

As discussed by Poll and Hunt [16], the spherical components in a space-fixed coordinate system of the induced dipole moment for a pair of molecules can be written quite generally in terms of appropriately coupled spherical harmonics

$$\mu_v(\mathbf{r}_1\mathbf{r}_2\mathbf{R}) = [(4\pi)^3/3]^{1/2} \sum_{\lambda_1\lambda_2\Lambda L} A_\Lambda(\lambda_1\lambda_2 L; r_1 r_2 R) \sum_{\mu_1\mu_2 M} C(\Lambda L 1; \mu_1+\mu_2, M, v) \quad C(\lambda_1\lambda_2\Lambda; \mu_1, \mu_2, \mu_1+\mu_2) Y_{\lambda_1\mu_1}(\omega_1)\, Y_{\lambda_2\mu_2}(\omega_2) Y_{LM}(\Omega). \quad (1)$$

In this expression, $\mathbf{r}_1$ ($= r_1, \omega_1$) and $\mathbf{r}_2$ ($= r_2, \omega_2$) are the vectors describing the orientation of the internuclear axes of molecules 1 and 2, respectively, and $\mathbf{R}$ ($\equiv R, \Omega$) is the vector separation between their centers of mass; the C's are Clebsch–Gordan coefficients and the Y's are spherical harmonics. The dipole coefficients, $A_\Lambda(\lambda_1\lambda_2 L; r_1 r_2 R)$, are real functions of the radial variables and provide a coordinate-independent representation of the strength of the various induction mechanisms specified by the indices λ_1, λ_2, Λ and L. Explicit results for $A_\Lambda(\lambda_1\lambda_2 L; r_1 r_2 R)$ arising from quadrupolar ($L = 3$) and hexadecapolar ($L = 5$) induction are given in Table 1. In addition, there are weaker components arising from a quadrupole moment on one molecule inducing a dipole on a second molecule, and then this induced-dipole induces a dipole back on the first molecule; this was called a "back reaction" in Ref. [15]. The long-range coefficients having $L = 1$ are also displayed in Table 1. For each component in Table 1, there is also a short-range part that we model by adding a term $\mu_L e^{-(R-\sigma)/\rho}$, where μ_L ($L = 1,3,5$) are adjustable parameters, σ is the Lennard–Jones radius, and ρ is a range parameter which we arbitrarily choose as $\rho = 0.11\sigma$, a value that has been used previously to model H_2 collision-induced spectra.

Table 1

λ_1	λ_2	Λ	L	$A_\Lambda(\lambda_1\lambda_2 L; r_1 r_2 R)$
0	0	0	1	$6/5[\alpha(r_1)\gamma(r_2)Q_2(r_2) - \alpha(r_2)\gamma(r_1)Q_2(r_1)]R^{-7}$
2	0	2	1	$\sqrt{2}/5[(9\alpha(r_1) + 3\gamma(r_1))\alpha(r_2)Q_2(r_1) - \gamma(r_1)\gamma(r_2)Q_2(r_2)/5]R^{-7}$
0	2	2	1	$-\sqrt{2}/5[(9\alpha(r_2) + 3\gamma(r_2))\alpha(r_1)Q_2(r_2) - \gamma(r_1)g(r_2)Q_2(r_1)/5]R^{-7}$
2	0	2	3	$\sqrt{3}\,[Q_2(r_1)\alpha(r_2)]R^{-4}$
0	2	2	3	$-\sqrt{3}\,[\alpha(r_1)Q_2(r_2)]R^{-4}$
2	2	2	3	$-(2/105)^{1/2}\,[Q_2(r_1)\gamma(r_2) - Q_2(r_2)\gamma(r_1)]R^{-4}$
2	2	3	3	$-(2/15)^{1/2}\,[Q_2(r_1)\gamma(r_2) + Q_2(r_2)\gamma(r_1)]R^{-4}$
2	2	4	3	$-3(2/35)^{1/2}\,[Q_2(r_1)\gamma(r_2) - Q_2(r_2)\gamma(r_1)]R^{-4}$
4	0	4	5	$\sqrt{5}\,[Q_4(r_1)\alpha(r_2)]R^{-6}$
0	4	4	5	$-\sqrt{5}\,[\alpha(r_1)Q_2(r_2)]R^{-6}$
4	2	4	5	$-2/3(7/55)^{1/2}\,[Q_4(r_1)\gamma(r_2)]R^{-6}$
4	2	5	5	$-2(1/15)^{1/2}\,[Q_4(r_1)\gamma(r_2)]R^{-6}$
4	2	6	5	$-(26/33)^{1/2}\,[Q_4(r_1)\gamma(r_2)]R^{-6}$
2	4	4	5	$2/3(7/55)^{1/2}\,[\gamma(r_1)Q_4(r_2)]R^{-6}$
2	4	5	5	$-2(1/15)^{1/2}\,[\gamma(r_1)Q_4(r_2)]R^{-6}$
2	4	6	5	$(26/33)^{1/2}\,[\gamma(r_1)Q_4(r_2)]R^{-6}$

As in our previous paper [6] on N_2, we neglect the anisotropic interaction between the colliding molecules and write the absorption in terms of a superposition of components. Each component, n, is specified by the set of integers

$$n \equiv \{v_1, J_1, v_2, J_2, v_1', J_1', v_2', J_2', \lambda_1, \lambda_2, \Lambda, L\}. \tag{2}$$

where v and J are the vibrational and rotational quantum numbers, respectively. The strengths of the individual components at a temperature T are given by [16]

$$S_n(T) = P_{J_1}\, C(J_1\lambda_1 J_1'; 00)^2\, P_{J_2}\, C(J_2\lambda_2 J_2'; 00)^2\, \langle B_n(R)^2 \rangle, \tag{3}$$

in which

$$B_n(R) = \langle v_1 v_2 J_1 J_2 | A_\Lambda(\lambda_1\lambda_2 L; r_1 r_2 R) | v_1' v_2' J_1' J_2' \rangle \tag{4}$$

is the matrix element of the coefficient A between the initial and final vibration–rotational states of molecules 1 and 2 assuming simple product-type wavefunctions. The P_J are the normalized Boltzmann factors

$$P_J = g_J\,(2J+1)\,\mathrm{e}^{-E_J/kT}/Q(T), \tag{5}$$

where

$$Q(T) = \sum_J g_J\,(2J+1)\,\mathrm{e}^{-E_J/kT} \tag{6}$$

and for $^{16}O_2$ the statistical weights are $g_J = 0$ for even J and $g_J = 1$ for odd J. Because of the Boltzmann factors all the initial state vibrational quantum numbers are 0, and since we are interested in the fundamental spectrum, either v_1' or v_2' must equal 1. We arbitrarily assume molecule 2 makes the vibrational transition ($v_1' = 0$, $v_2' = 1$) and multiply our final expression for the absorption coefficient by 2. Therefore, using the explicit results for the induction coefficients $A_\Lambda(\lambda_1\lambda_2 L; r_1 r_2 R)$ listed in Table 1, we can write the $B_n(R)$ in the form

$$B_n(R) = \langle 00 J_1 J_2 | A_\Lambda(\lambda_1\lambda_2 L; r_1 r_2) | 01 J_1' J_2' \rangle\, R^{-(L+1+5\delta}L1), \tag{7}$$

where δ_{L1} is the Kronecker delta. The average over molecular orientations, denoted by angular brackets, can be calculated using the well-known results

$$\langle B_n(R)^2 \rangle = 4\pi \int_0^\infty B_n(R)^2\, g(R)\, R^2\, \mathrm{d}R, \tag{8}$$

where $g(R)$ is the pair distribution function and all quantities in the integrand are in atomic units. In the low-density classical limit, and considering only the isotropic interaction (i.e., neglecting the multipolar and other anisotropic interactions), $g(R)$ may be written

$$g(R) = \mathrm{e}^{-V_0(R)/kT}, \tag{9}$$

where we assume that the isotropic potential $V_0(R)$ can be adequately represented by a Lennard–Jones potential having the parameters $\varepsilon/k = 106.7$ K and $\sigma = 6.55\, a_0$. Furthermore, if we neglect the slight dependence of the matrix elements in Eq. (7) on the rotational quantum numbers, we can approximate Eq. (8) by

$$\langle B_n(R)^2 \rangle \cong |\langle 0000 | A_\Lambda(\lambda_1\lambda_2 L; r_1 r_2) | 0100 \rangle|^2\, I(L), \tag{10}$$

where

$$I(L) = 4\pi \int_0^\infty R^{-2(L+5\delta L1)} \, \mathrm{e}^{-V_0(R)/kT} \, \mathrm{d}R \tag{11}$$

and $L = 1$, 3 or 5 for the back, quadrupolar, and hexadecapolar induction mechanisms, respectively.

3. Modeling of the line shape

Each component $\{\lambda_1\lambda_2\Lambda L\}$ of the induced dipole gives rise to a large number of closely spaced transitions and since we have assumed isotropic interactions in the previous section, the various lines are additive. For synthesizing the induced spectrum each vibration–rotational transition is modeled by a line shape that is broadened by the translational motion. To our knowledge, no quantum line shapes, $L_j(\omega - \omega_0)$, where j indicates the induction mechanism, similar to those given by Borysow and Frommhold [17] for N_2 have been published for O_2. Therefore, we use those for N_2, modified to account for the appearance of an intercollisional dip

$$L'_j(\omega - \omega_0) = \left[1 - \frac{\gamma}{(\omega - \omega_0)^2/r^2 + 1}\right] L_j(\omega - \omega_0), \tag{12}$$

where $0 \leq \gamma \leq 1$ is a density-independent parameter corresponding to the depth of the dip at the center frequency ω_0, and Γ is a density-dependent parameter describing the width of the dip.

We have arbitrarily assumed that molecule 2 makes the vibrational transition and in this case the frequency for the transition $f <- i$ can be approximated by

$$\begin{aligned}\omega_{if} \cong\, & \nu_{01} + B_0[J'_1(J'_1+1) - J_1(J_1+1)] - D_\mathrm{e}[J'^2_1(J'_1+1)^2 - J^2_1(J_1+1)^2] \\ & + B_1[J'_2(J'_2+1)] - B_0[J_2(J_2+1)] - D_\mathrm{e}[J'^2_2(J'_2+1)^2 - J^2_2(J_2+1)^2],\end{aligned} \tag{13}$$

where ν_{01} is the fundamental band-center frequency, and B_v and D_e are the usual rotational parameters. The values (in cm^{-1}) used are: $\nu_{01} = 1556.38$, $B_0 = 1.4377$, $B_1 = 1.4219$, and $D_\mathrm{e} = 4.8 \times 10^{-6}$. The rotational quantum numbers J_1 and J_2 take the values 0, 1, 2, …, subject to the selection rules:

$$\begin{aligned}J'_1 &= J_1 + \lambda_1, J_1 + \lambda_1 - 2, \ldots, |J_1 - \lambda_1|, \\ J'_2 &= J_2 + \lambda_2, J_2 + \lambda_2 - 2, \ldots, |J_2 - \lambda_2|.\end{aligned} \tag{14}$$

If $L'_j(\omega - \omega_{if})$ represents the modified line shape for the transition $f <- i$, then the absorption coefficient $\alpha(\omega)$ divided by the square of the density ρ in amagats can be written in the form [16]

$$A(\omega, T) \equiv \alpha(\omega)/\rho^2 = (4\pi^2/3)\,\alpha_\mathrm{F} n_0^2 a_0^5 \omega \sum_{\substack{j, J_1, J'_1 \\ J_2, J_2}} S_J(T) L'_j(\omega - \omega_{if}), \tag{15}$$

where α_F is the fine-structure constant ($\cong \frac{1}{137}$), n_0 is the number density at normal temperature and pressure, and a_0 is the Bohr radius.

4. Polarizability and multipolar parameters

As in the case of nitrogen, the main induction mechanism is quadrupolar, with the hexadecapolar and back-reaction mechanisms contributing only a small amount to the intensity. The induced dipole $\boldsymbol{\mu}$ of one molecule due to the multipolar electric field E of another is of the form

$$\boldsymbol{\mu} = \boldsymbol{\alpha}\mathbf{E} + \gamma\mathbf{E}, \tag{16}$$

where α and γ are the isotropic and anisotropic parts, respectively, of the polarizability tensor. We can expand these functions in a Taylor series about the equilibrium internuclear separation r_e in order to calculate the matrix elements:

$$\alpha(r) = \alpha(r_e) + (\partial\alpha/\partial r)_{r_e}(r - r_e) + \cdots, \tag{17a}$$

$$\gamma(r) = \gamma(r_e) + (\partial\gamma/\partial r)_{r_e}(r - r_e) + \cdots, \tag{17b}$$

$$Q(r) = Q(r_e) + (\partial Q/\partial r)_{r_e}(r - r_e) + \cdots, \tag{17c}$$

and

$$\Phi(r) = \Phi(r_e) + (\partial\Phi/\partial r)_{r_e}(r - r_e) + \cdots. \tag{17d}$$

We now discuss the choices we adopted for the corresponding matrix elements.

4.1. Polarizability matrix elements

Considering the importance in phenomena such as absorption, refraction, light scattering, and intermolecular forces, the molecular dipole polarizability has received much attention both experimentally and theoretically.

Since the pioneering calculations of Werner and Meyer [18] in 1976, the ab initio calculation of static second-order molecular properties has approached the best experimental accuracy in several cases. Hettema et al. [19] computed the dipolar and quadrupolar polarizabilities of molecular oxygen in its $^3\sum_g^-$ ground state by means of the multiconfiguration self-consistent field method with different basis sets. The restricted active space (RAS) gives good agreement with experimental values and other calculations. A recent experimental value

$$\alpha_{00} \equiv \langle v = 0|\alpha(r)|v = 0\rangle = (10.87 \pm 0.20)\, a_0^3 \tag{18}$$

was obtained by Buldakov et al. [20] from a measurement where the treatment of experimental data took into account the mechanical and electro-optical anharmonicities and the vibration–rotational interaction that were shown to be negligible. Another experimental value ($10.66a_0^3$) [21] is in good agreement with the experimental value ($10.75a_0^3$) for the average polarizability [22], and consistent with the older value ($10.78a_0^3$) of Bridge and Buckingham [23]. More recently, Hohm and Kerl [24] obtained the same value in precise monochromatic measurements at $\lambda = 632.99$ nm using interferometric methods. In the present work, we assume the value for $\alpha_{00} = 10.87a_0^3$.

Buldakov et al. [20] also reported a value for the anisotropic part of the polarizability; they reported

$$\gamma_{00} \equiv \langle v = 0|\gamma(r)|v = 0\rangle = (7.30 \pm 0.27)a_0^3 \tag{19}$$

which we also adopt in the present work. This value is in good agreement with a previous experimental value ($7.43a_0^3$) by Bridge and Buckingham [25] obtained at 632.8 nm. The best value for the recent RAS ab initio calculation of Hettema et al. [19] is $7.157a_0^3$, very close to the earlier ab initio value by Rijks et al. [26] who used an entirely different method.

Polarizability gradients have been obtained experimentally only in a few studies. Comparison of results shows that values obtained for the derivative of the isotropic polarizability are in good agreement, but that is not the case for the anisotropic component. In the present work, we adopt the value

$$\alpha_{01} \equiv \langle v=0|\alpha(r)|v=1\rangle \cong r_e(B_e/\omega_e)^{1/2}(\mathrm{d}\alpha/\mathrm{d}r)_{r_e}$$
$$= (0.357 \pm 0.002)a_0^3, \tag{20}$$

based on the measurement of the absolute values of the differential scattering cross-sections for individual lines in the O- and S-branches of the fundamental Raman spectra by Buldakov et al. [20]. We used the following spectroscopic constants: $r_e = 1.20752$ Å, $B_e = 1.44563\,\mathrm{cm}^{-1}$, and $\omega_e = 1580.193\,\mathrm{cm}^{-1}$. This value for α_{01} is in good agreement with an earlier determination of $0.343a_0^3$ by Stansbury et al. [27].

We derived the vibrational matrix element of the anisotropic polarizability from an evaluation of the gradient about the equilibrium internuclear separation, r_e, by means of a polynomial fitting of the ab initio data of Hettema et al. [19]. This fit yields

$$\gamma_{01} \equiv \langle v=0|\gamma(r)|v=1> \cong r_e(B_e/\omega_e)^{1/2}(\mathrm{d}\gamma/\mathrm{d}r)_{r_e}$$
$$= 0.57a_0^3, \tag{21}$$

but is lower than the experimental value $(0.650 \pm 0.05)a_0^3$ of Stansbury et al. [27]. From measurements of small changes in the relative intensity of different vibration–rotational Raman transitions, Asawaroengchai and Rosenblatt [28] reported a much higher value of $(0.95 \pm 0.30)\ a_0^3$. In the present work, we use the value in Eq. (21).

4.2. Electric multipole moment matrix elements

The restrictive active space (RAS) electric quadrupole moment of Hettema et al. [19] ($-0.264ea_0^2$) lies between the experimental values [29, 30] of ($-0.299ea_0^2$) and ($-0.25 \pm 0.01)ea_0^2$ and is not far from the ab initio value ($-0.271ea_0^2$) of Rijks et al. [26]. Another MCSF calculation by van Lenthe and van Duijneveldt [31] is close to the RAS value, while that obtained by Evans [32] ($-0.223ea_0^2$) from the best fit to the experimental intensity and band shape of the collision-induced rotation- translation band measured by Bosomworth and Gush [33] is lower. In the present work, we adopt the RAS value

$$Q_{00} = \langle v=0|Q(r)|v=0\rangle = -0.264ea_0^2. \tag{22}$$

In addition to the quadrupole induction mechanism, we also consider the hexadecapolar mechanism. Several semiempirical estimates [31, 32, 34] have been given with values ranging between 2.945 and $21.242ea_0^4$. In the following, we assume the RAS value [19]

$$\Phi_{00} \equiv \langle v=0|\Phi(r)|v=0\rangle = 4.4ea_0^4. \tag{23}$$

This is in excellent agreement with the ab initio results of Rijks et al. [26], but approximately 10% higher than the value ($4.087ea_0^4$) of Visser [35] who used a similar method, but did not include triple excitations in the CI wave function.

Using the same procedure that we used for α_{01} and γ_{01}, we obtained from interpolation of the multipolar function at several internuclear separations calculated by Hettema et al. [19] the values

$$Q_{01} \equiv \langle v=0|Q(r)|v=1\rangle \cong r_e(B_e/\omega_e)^{1/2}\,(\mathrm{d}Q/\mathrm{d}r)_{r_e}$$
$$= 0.106ea_0^2 \tag{24}$$

and

$$\Phi_{01} \equiv \langle v=0|\Phi(r)|v=1\rangle \cong r_e(B_e/\omega_e)^{1/2}\,(\mathrm{d}\Phi/\mathrm{d}r)_{r_e}$$
$$= 0.185ea_0^4. \tag{25}$$

that we use in the calculations. It should be noted that the value adopted for Q_{01} is in excellent agreement with that derived by Shapiro and Gush [36] from the quadrupole contribution to the collision-induced fundamental spectrum.

5. Results

Using the theory outlined in Section 2, the line shape described in Section 3, and the values for the matrix elements given in Section 4, we have calculated the spectra for five temperatures between 193 and 273 K; the results with $\gamma = 0$ (i.e., no intracollisional dips) for 193 and 273 K are compared with the experimental spectra in Figs. 1a and b, respectively. As can be seen there, the theoretical spectra are in good agreement with the experimental spectra within the experimental error bars shown on the figures. The percentage difference between theory and experiment are plotted in Fig. 2 for five temperatures, where it can be seen that these are systematic, being much larger in the wings where the experimental intensities are lower and the corresponding error bars larger. A similar effect was found in N_2 [6]. In order to examine the role of the three different induction mechanisms, we plot in Fig. 3 the contributions separately for (a) $T = 193$ K, and (b) $T = 273$ K. It is apparent that in the center of the band, the quadrupole mechanism ($L = 3$) dominates. More specifically, the $Q_{01}\alpha_{00}$ mechanism accounts for approximately 90% of the absorption in the present case, whereas it contributed approximately 75% in the case of N_2 –N_2. As one gets into the wings of the band, the hexadecapolar mechanism ($L = 5$) increases in importance as expected because of the different selection rules and the broader line widths. The back-reaction mechanism ($L = 1$) makes a negligible contribution at all frequencies.

As mentioned above, we have assumed in the present calculations, the same line shapes as for N_2 [17]. In order to test the sensitivity of the total profile to the line shape, we have varied the parameter $\tilde{\tau}_1$ appearing in the theoretical representation by $\pm$ 20% and show the results in Fig. 4. The influence on the global fit is illustrated in Fig. 5a, and for three different regions with expanded intensity scales in Fig. 5b–d. In the Q branch, the larger value of τ_1 gives a better fit to the experiment. However, this is not true in the plateau region of the S branch, where this line shape produces the worst agreement. None of the three line shapes is capable of producing enough absorption in the high-frequency far wing of the band.

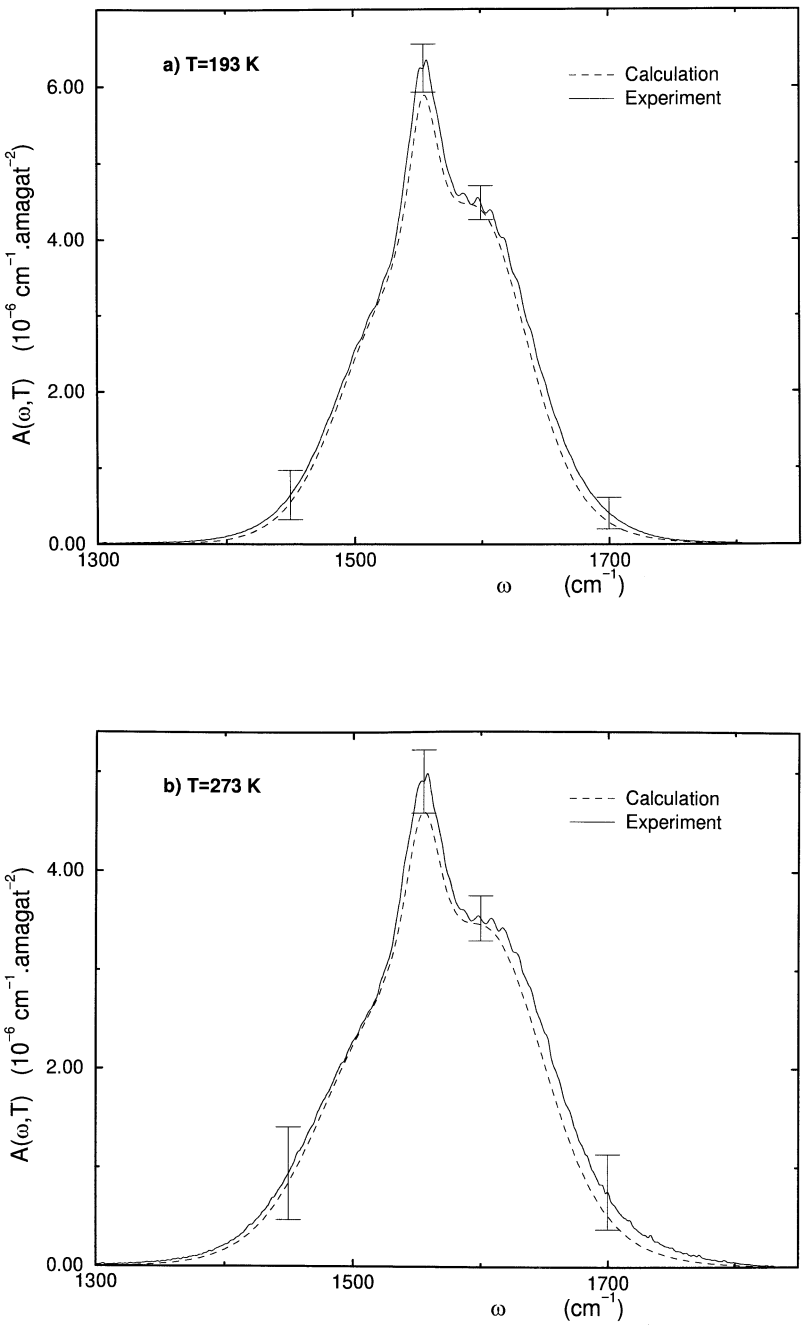

Fig. 1. Comparison between theory and experiment for the absorption coefficient (in units 10^{-6} cm^{-1} amagat^{-2} versus frequency ω in cm^{-1} for the O_2 fundamental band: (a) $T = 193$ K; (b) $T = 273$ K.

In order to test the sensitivity to the choice of the dominant matrix elements, we plot in Figs. 6 and 7, the profiles obtained with different choices of Q_{01} and α_{00}, respectively, one slightly larger and the other slightly smaller than the "best" values we assumed from the literature. These do not improve the agreement; in fact, in the plateau region, the values chosen provide the best agreement.

We can also vary the coefficient of the short-range part of the various dipole components μ_L. Because the $L = 1$ contribution was found to be negligible, we show in Fig. 8 the results calculated by varying μ_3. One can get somewhat better fits in the plateau region by choosing $\mu_3 = -2 \times 10^{-5}$, but the global fits are not improved appreciably; similar conclusions obtain for μ_5.

In an attempt to elucidate the origin of the small structural features, we have drawn a smooth curve through the peaks of the absorption features in the plateau region, $A(\omega, T)_{\max}$, and have divided this by the experimental value $A(\omega, T)_{\exp}$. Results for three densities at $T = 252$ K are given

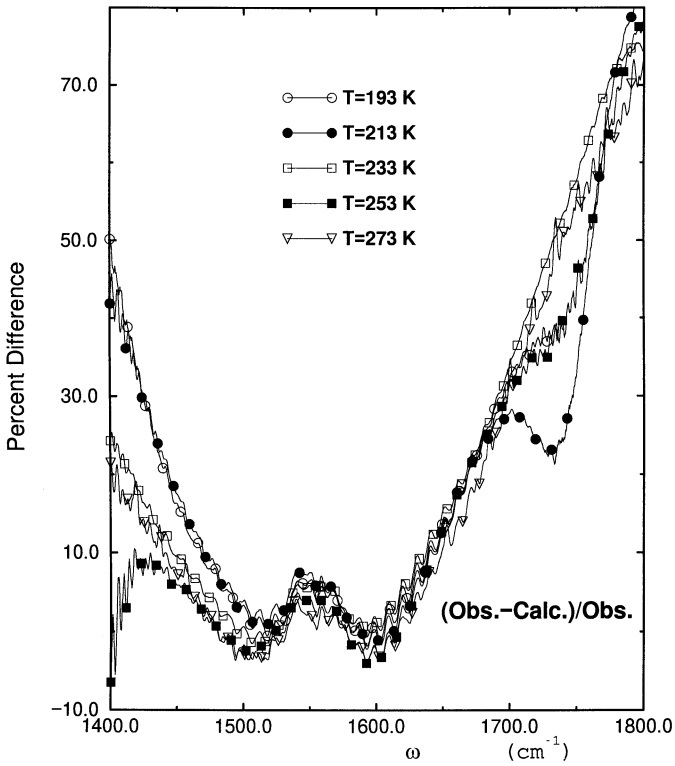

Fig. 2. The percent difference between theory and experiment for five temperatures as a function of frequency ω in cm^{-1}.

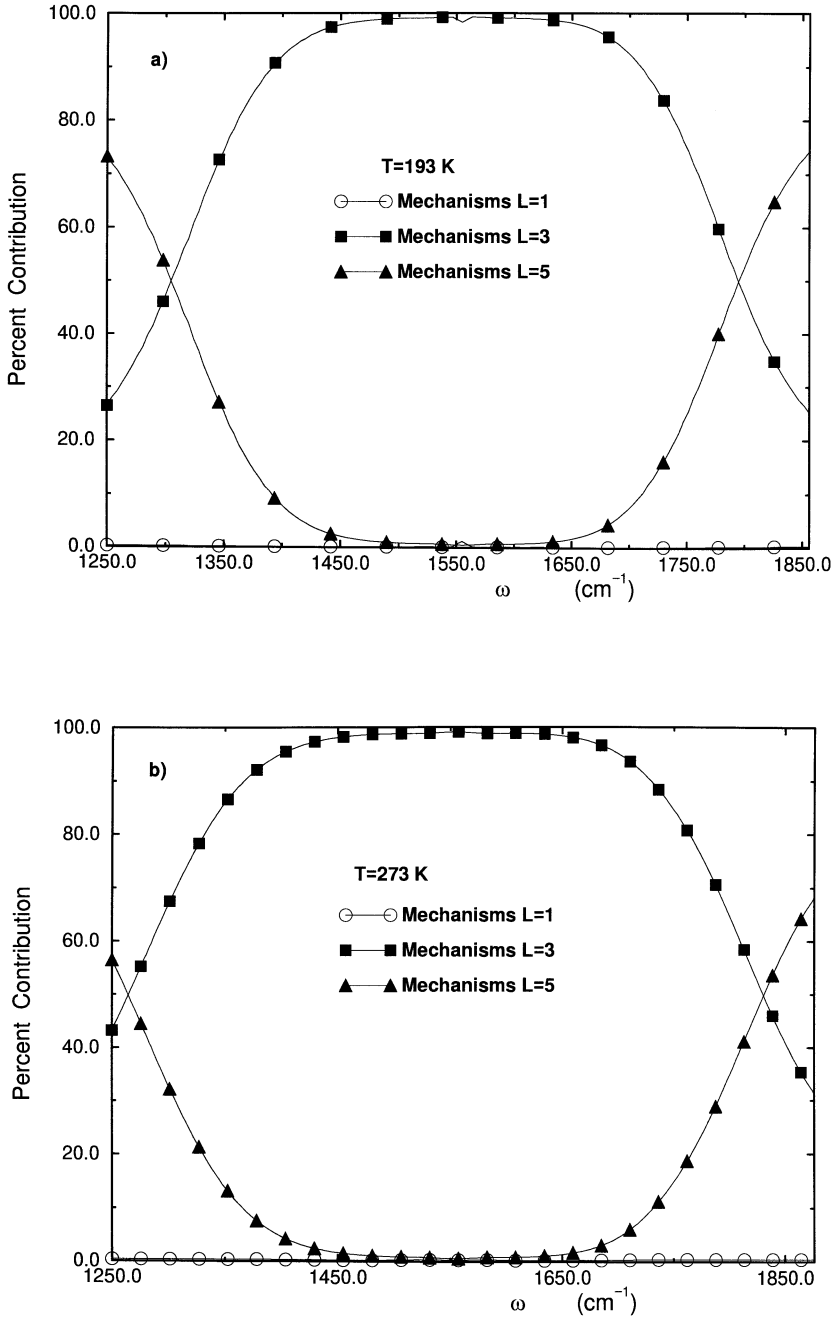

Fig. 3. The percent contribution to the theoretical absorption as a function of frequency for the three induction mechanisms $L = 1$, 3, and 5: (a) $T = 193$ K; (b) $T = 273$ K.

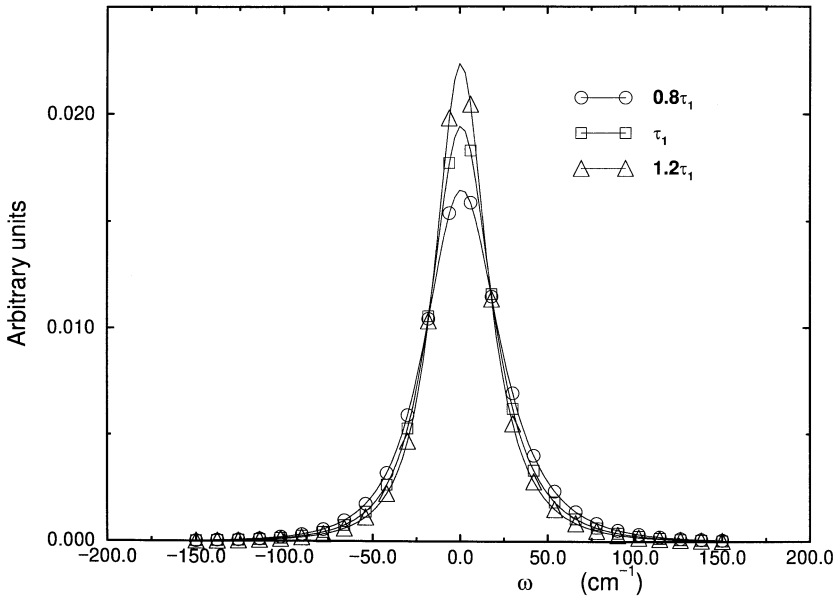

Fig. 4. The theoretical collision-induced line shape as a function of the parameter τ_1.

by the solid curves in Fig. 9, where it can be seen that the dips (the peaks in these figures) occur at the Raman transitions indicated by the vertical lines. We then attempted to fit these curves by varying γ and Γ in Eq. (12). The best overall fit, shown by the dashed lines in Fig. 9 was obtained for $\gamma = 0.2$ and $\Gamma(\mathrm{cm}^{-1}) = 2.715 + 0.133\rho$, where ρ is the density in amagats. If the origin of the features were intracollisional interference, one would expect Γ to be proportional to ρ, since the area of the dips should vary as the density cubed [12]. The constant width at $\rho = 0$ would tend to rule out this interpretation.

In Fig. 10, we show the results obtained by subtracting the theoretical spectra calculated with the "best" parameters from the observed results at a fixed density ($\rho = 6.8$ amagats) but for two different temperatures ($T = 193$ and 273 K); the Raman O, Q, and S transition frequencies are given for reference. These results are very similar to those obtained by McKellar at low temperatures for the fundamental band of N_2–N_2, and are consistent with the dimer interpretation given by Long et al. [37].

6. Discussion and conclusions

From the results presented above, we can draw the following conclusions. First of all, the overall fit to the collision-induced fundamental band of O_2–O_2 can be calculated with reasonable accuracy for different temperatures and densities using only the long-range quadrupolar and hexadecapolar mechanisms. The "best" values for the matrix elements of the isotropic and anisotropic polarizability, and for the quadrupole and hexadecapole moments give the best global fit to the experimental spectral profiles. Introducing short-range components whose magnitude can be parameterized

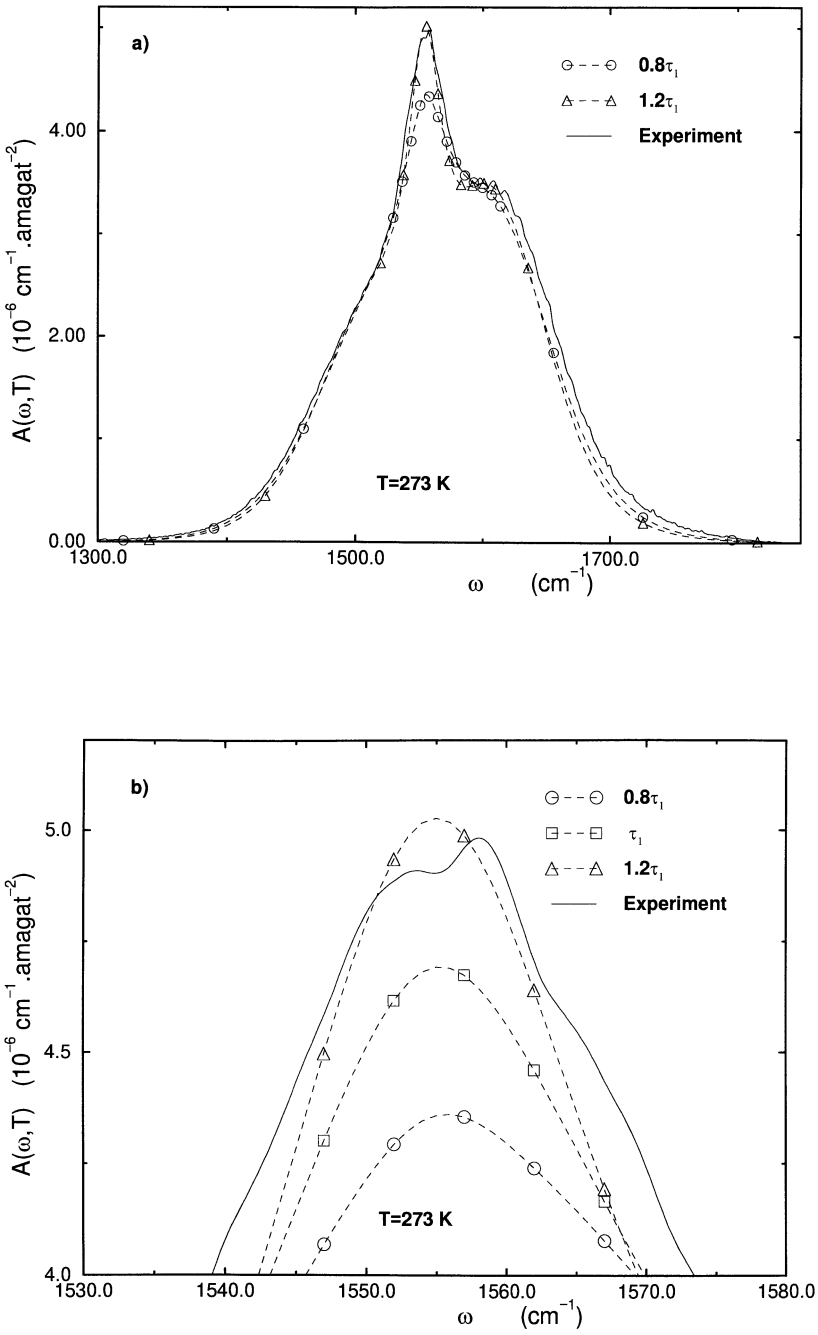

Fig. 5. The influence of variations in the line-shape parameter τ_1 on the spectrum at $T = 273$ K: (a) The global fit; (b) The Q-branch region; (c) The plateau region of the S branch; (d) The high-frequency far-wing region.

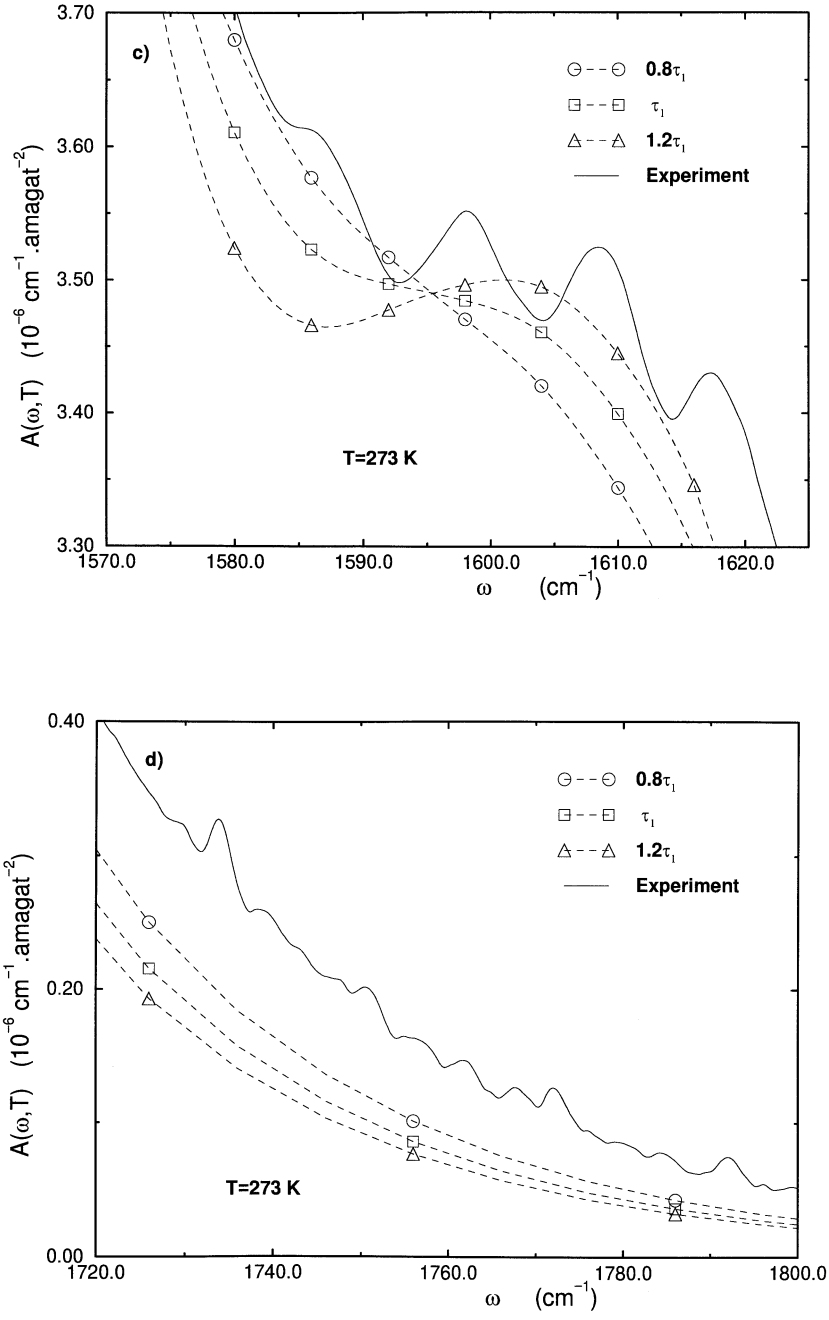

Fig. 5. (*continued*).

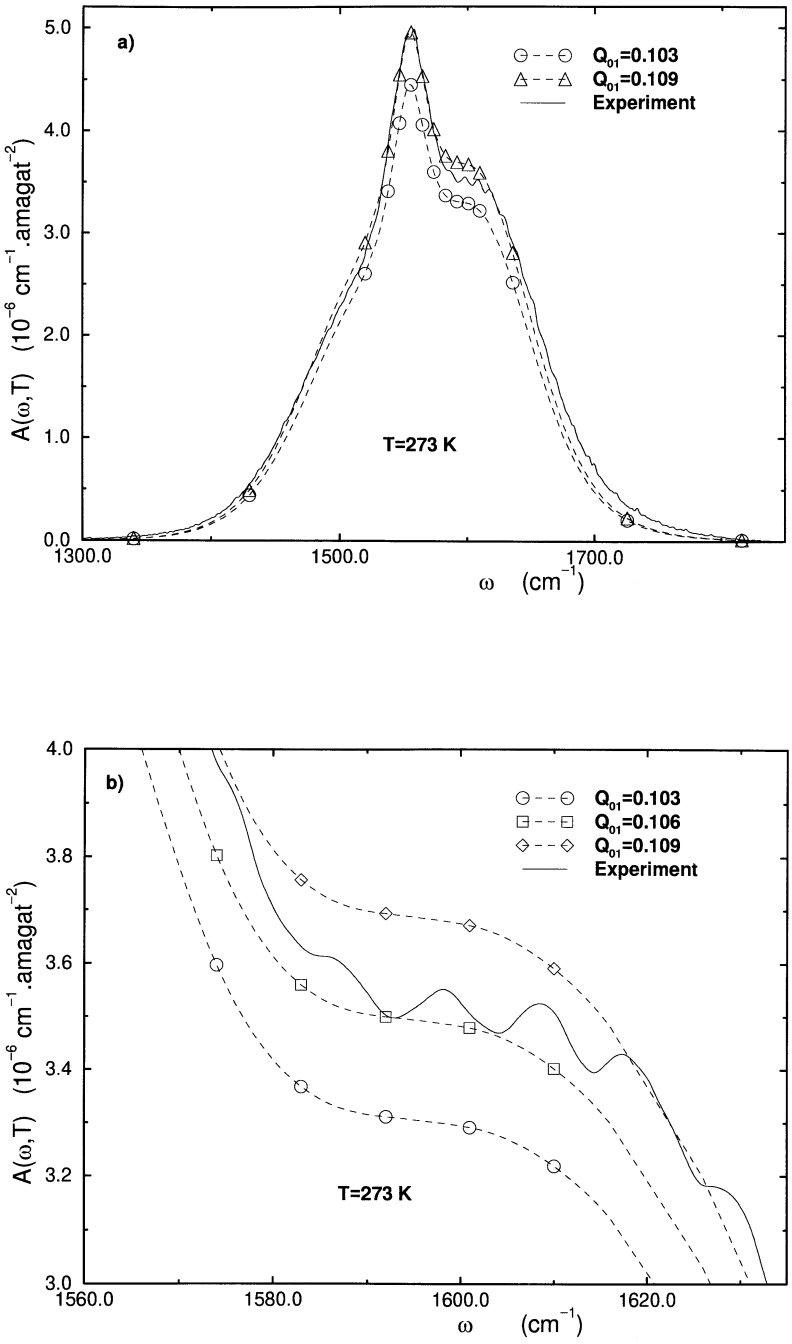

Fig. 6. The influence of variations of the quadrupole moment matrix element, Q_{01}, on the spectrum at $T = 273$ K: (a) The global fit; (b) The plateau region of the S branch.

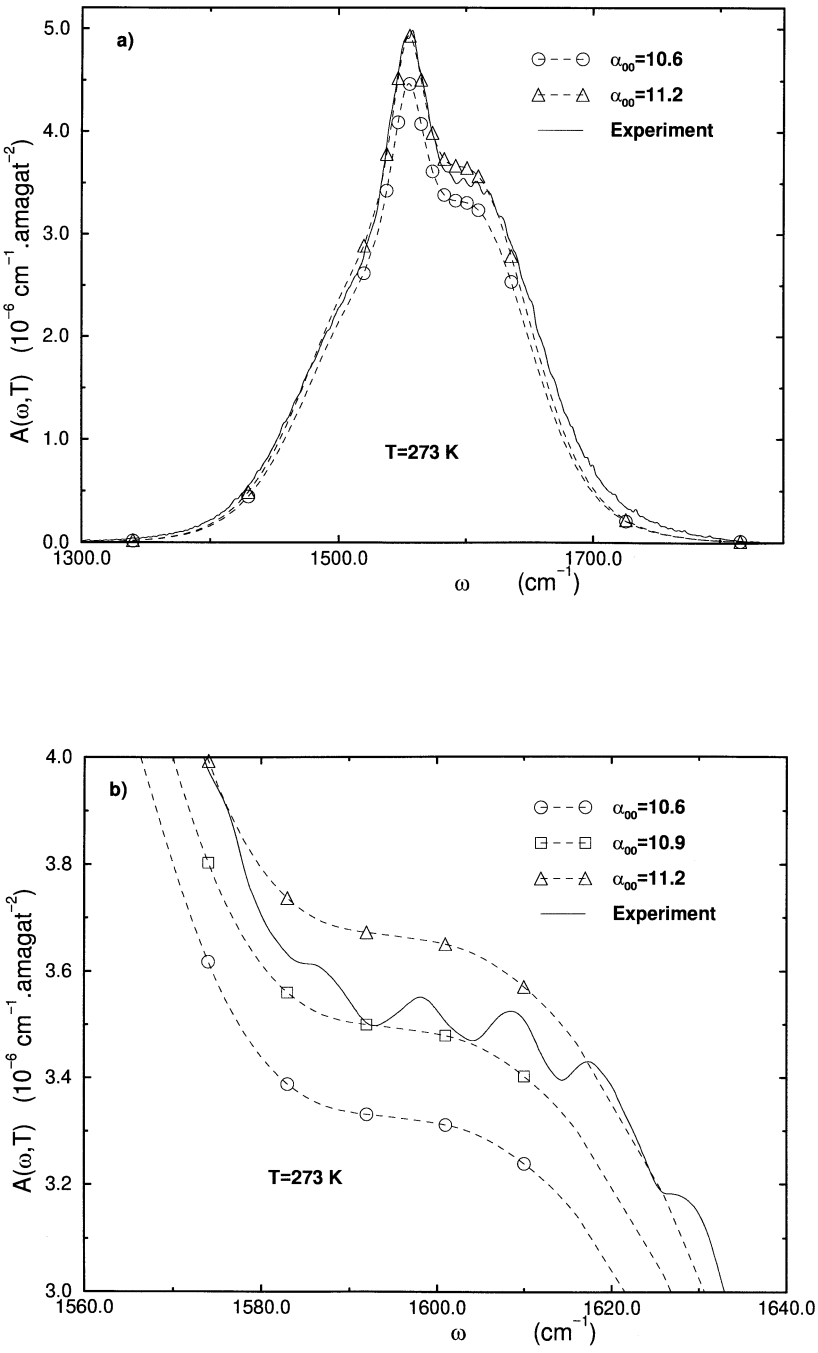

Fig. 7. The influence of variations of the isotropic polarizability matrix element, α_{00}, on the spectrum at $T = 273$ K: (a) The global fit; (b) The plateau region of the S branch.

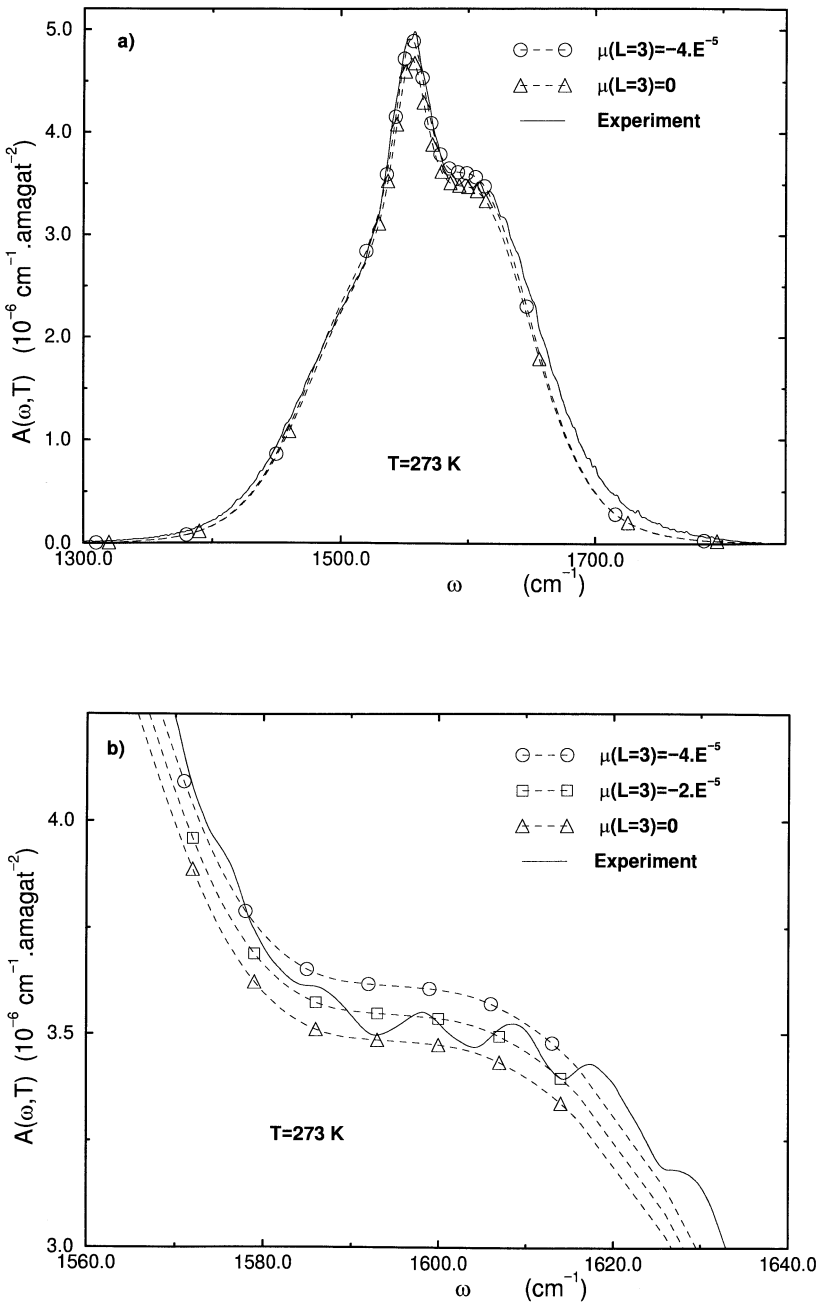

Fig. 8. The influence of short-range induction mechanism for $L = 3$ on the spectrum at $T = 273$ K: (a) The global fit; (b) The plateau region of the S branch.

does not produce noticeable overall improvement, but it can change the agreement in limited spectral regions; i.e., in the peak of the Q-branch, or in the plateau region of the S branch. In general, in the far wings of the band the experimental absorption is greater than the theoretical calculations. This would seem to indicate that higher-order multipolar induction that will contribute relatively more in the wings may be required to fit these region. Similar discrepancies in the high-frequency wings of the rotation- translational Raman spectra of N_2 have been reported and attributed by some workers to a large "dipole–octopole" polarizability [38], while other workers [39] attribute this to normal pressure broadening.

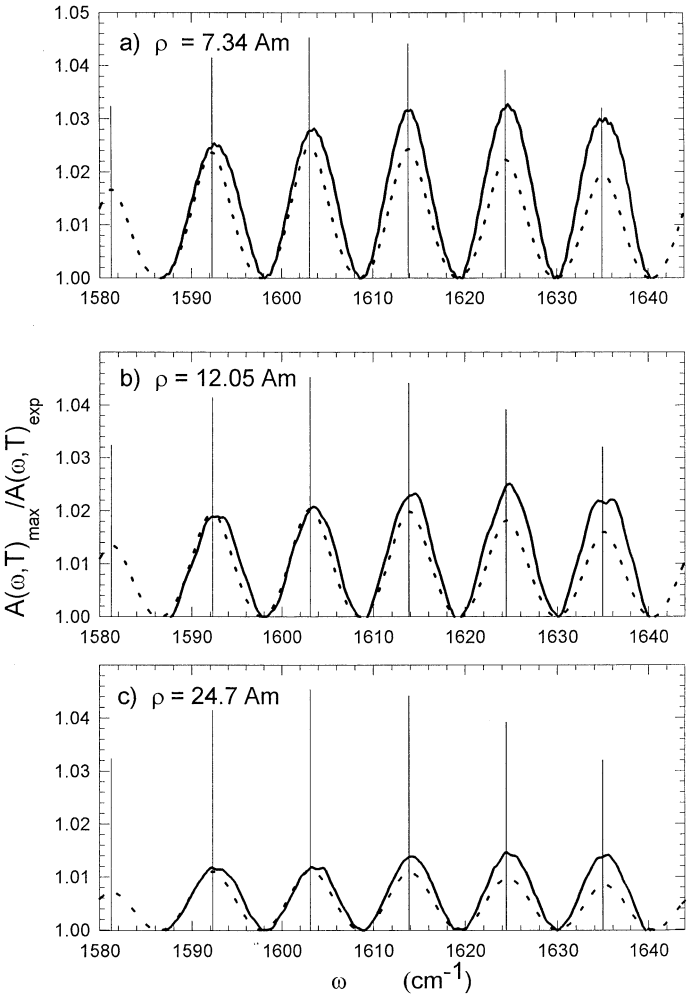

Fig. 9. The ratio $A(\omega, T)_{max}/A(\omega, T)_{exp}$ versus frequency ω given by the solid curves at $T = 252$ K for several densities ρ: (a) 7.34 amagats; (b) 12.05 amagats; (c) 24.7 amagats. The dashed curve is the best fit with $\gamma = 0.2$ and $\Gamma = 2.715 + 0.133\rho$.

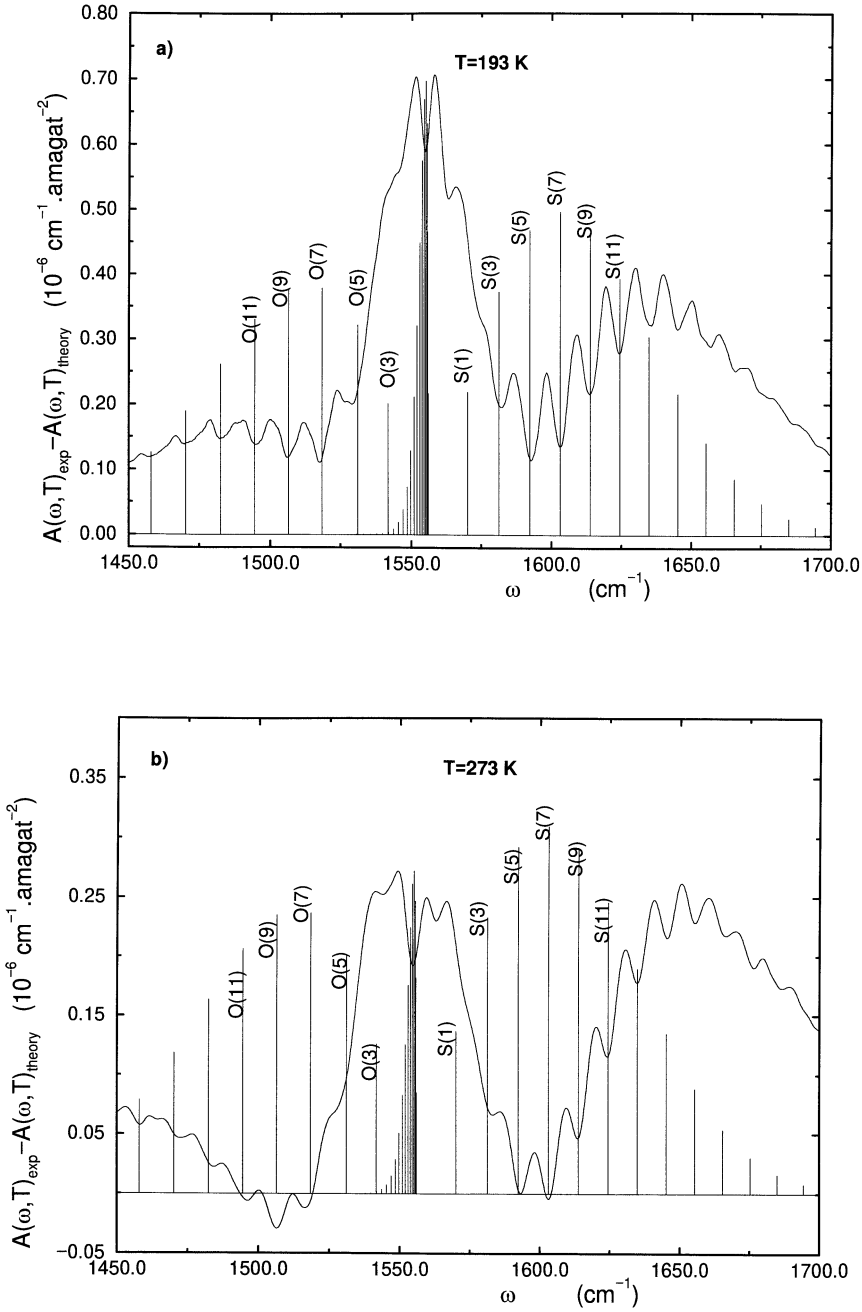

Fig. 10. The residual spectrum obtained after subtraction the best fit theoretical spectrum from the experimental result: (a) $T = 193$ K; (b) $T = 273$ K. The first few Raman transitions are labeled.

By introducing a parameterized line shape to model the effects of intercollisional interference, we were able to obtain reasonable fits to the small structural features most apparent in the plateau region; however, the density dependence obtained for Γ is not in agreement with that expected for this mechanism. Furthermore, by subtracting out the smooth theoretical absorption from the experimental data, the residual spectra look very similar to those obtained at low temperature for N_2–N_2 pairs and attributed to dimers.

Further experimental work, especially at higher temperature, in the pure rotational and fundamental bands would be useful to verify that the observed structure in the spectra of both N_2–N_2 and O_2–O_2 pairs is indeed due to dimers. Finally, it would also be worthwhile to consider, experimentally and theoretically, the pure rotational and fundamental bands of O_2–N_2 and N_2–O_2 mixtures, and theoretical work on these systems is in progress.

Acknowledgements

Two of the authors (RHT and QM) would like to acknowledge support from NASA through Grants NAGW-4693 and NAG5-6314, and three authors (CB, RHT, and QM) wish to thank NATO for an exchange Grant (CRG 940247) that greatly facilitated this research.

References

[1] Crawford MF, Welsh HL, Locke JL. Phys Rev 1949;80:607.
[2] Frommhold L. *Collision-induced Absorption in Gases*. Cambridge: Cambridge University Press, 1993.
[3] Rich NH, McKellar ARW. Can J Phys 1976;54:486.
[4] Hunt JL, Poll JD. Mol Phys 1986;59:163.
[5] Rinsland P, Smith MAH, Seals Jr. RK, Goldman A, Murcray FJ, Murcray DG, Larsen JC, Rarig PL. J Geophys Res 1982;87:3119.
[6] Boissoles J, Tipping RH, Boulet C. JQSRT 1994;51:615.
[7] Lafferty WJ, Solodov AM, Weber A, Olson WB, Hartmann J-M. Appl Opt 1996;35:5911.
[8] McKellar ARW. J Chem Phys 1988;88:4190.
[9] Wishnow EH, Gush HP, Ozier I. J Chem Phys 1996;104:3511.
[10] Orlando JJ, Tyndall GS, Nickerson KE, Calvert JG. J Geophys Res 1991;96:20 755.
[11] Thibault F, Menoux V, Le Doucen R, Rosenmann L, Hartmann J.-M, Boulet C. Appl Opt 1997;36:1.
[12] van Kranendonk J. Can J Phys 1968;46:1173.
[13] Levy A, Lacome N, Chackerian Jr. C. In: Rao KN, Weber, A. editors. Spectroscopy of the atmosphere and interstellar medium. San Diego: Academic Press, 1992.
[14] Hunt JL. *The pressure-induced vibrational specture of hydrogen in the temperature range* 300 *to* 40 *K*. Dissertation, University of Toronto, 1959.
[15] Bohr JE, Hunt KLC. J Chem Phys 1987;87:3821.
[16] Poll JD, Hunt JL. Can J Phys 1976;54:461.
[17] Borysow A, Frommhold L. Astrophys J 1986;311:1043.
[18] Werner HJ, Meyer W. Mol Phys 1976;31:855.
[19] Hettema H, Wormer PES, Jorgensen P, Jensen HJ Aa, Helgaker T. J Chem Phys 1994;100:1297.
[20] Buldakov MA, Korolev BV, Matrosov II, Popova TN. Opt Spectrosc 1987;62:519; 1987;62:758; 1987;63:775.
[21] Newell AC, Baird RC. J Appl Phys 1965;36:3751.
[22] Koide A, Kihara T. Chem Phys 1974;5:34.
[23] Bridge NJ, Buckingham AD. J Chem Phys 1964;40:2733.

[24] Hohm U, Kerl K. Mol. Phys. 1990;69:803.
[25] Bridge NJ, Buckingham AD. Proc Roy Soc London A 1966;295:334.
[26] Rijks W, van Heeringen M, Wormer PES. J Chem Phys 1989;90:6501.
[27] Stansbury EJ, Crawford MF, Welsh HL. Can J Phys 1953;31:954.
[28] Asawaroengchai C, Rosenblatt GM. J Chem Phys 1980;72:2664.
[29] Buckingham AD, Disch RL, Dunmur DA. J Am Chem Soc 1968;90:3104.
[30] Cohen ER, Birnbaum G. J Chem Phys 1977;66:2443.
[31] van Lenthe JH, van Duijneveldt FB. J Chem Phys 1984;81:3168.
[32] Evans M. Mol Phys 1975;29:1345.
[33] Bosomworth DR, Gush HP. Can J Phys 1965;43:751.
[34] Sarangi S, Varanasi P. JQSRT 1974;14:989.
[35] Visser F, Wormer PES, Jacobs WPJH. J Chem Phys 1985;82:3753.
[36] Shapiro MM, Gush HP. Can J Phys 1966;44:949.
[37] Long CA, Henderson G, Ewing GE. Chem Phys 1973;2:485.
[38] Le Duff Y, Bancewitz T, Glaz W. In: Tabisz G, Neuman MN, editors. Collision- and interaction-induced spectroscopy, NATO advanced research workshops. Dordrecht: Kluwer, 1994.
[39] Fu Y, Borysow A, Moraldi M. Phys Rev A 1996;53:201.